TOPICAL REVIEW — Quantum information

Progress in superconducting qubits from the perspective of coherence and readout*

Zhong You-Peng(钟有鹏)[a], Li Chun-Yan(李春燕)[a], Wang Hao-Hua(王浩华)[a]†, and Chen Yu(陈 宇)[b]‡

[a] *Department of Physics, Zhejiang University, Hangzhou* 310027, *China*
[b] *Department of Physics, University of California, Santa Barbara, CA* 93106, *USA*

(Received 15 October 2013)

Superconducting qubits are Josephson junction-based circuits that exhibit macroscopic quantum behavior and can be manipulated as artificial atoms. Benefiting from the well-developed technology of microfabrication and microwave engineering, superconducting qubits have great advantages in design flexibility, controllability, and scalability. Over the past decade, there has been rapid progress in the field, which greatly improved our understanding of qubit decoherence and circuit optimization. The single-qubit coherence time has been steadily raised to the order of 10 to 100 μs, allowing for the demonstration of high-fidelity gate operations and measurement-based feedback control. Here we review recent progress in the coherence and readout of superconducting qubits.

Keywords: superconducting qubit, Josephson junction, quantum non-demolition measurement, decoherence

PACS: 03.67.Lx, 03.65.Yz, 85.25.Cp **DOI:** 10.1088/1674-1056/22/11/110313

1. Introduction

Consisting of two superconducting electrodes separated by a thin insulating barrier, Josephson junctions serve as a building block for the superconductivity-related technology. Building superconducting qubits out of Josephson junctions, and scaling up for a quantum computer may constitute the most important and ambitious application of Josephson junctions. After the first experimental observation of the macroscopic quantum tunneling in Josephson junctions,[1,2] Anthony Leggett proposed the idea of creating macroscopic quantum coherence using superconducting devices.[3] One decade later, a superconducting charge qubit made its debut, with the demonstration of generating a quantum superposition state.[4] Since then, research on superconducting qubits has become an active field in condensed matter physics, combing forces from many aspects including quantum mechanics, materials science, and circuit engineering.[5–9] Today, with greatly improved performance in both the coherence[10–13] and control,[14,15] superconducting qubits have stood out from the competitors and become one of the most promising candidates for quantum information processing.[16]

For a long time, decoherence has been the limiting factor in the development of superconducting qubits. The current understanding is that spurious two-level state (TLS) defects in dielectrics or metal surface oxide may play a dominant role,[17] with additional contributions from other mechanisms such as nonequilibrium quasiparticles.[18,19] Removing TLS defects may appear to be a challenging materials problem. Recently superconducting qubits in a three-dimensional (3D)[11,12] or two-dimensional (2D)[13,20] resonator cavity have shown exceptionally long coherence times of 10 to 100 μs, as compared to the typical gate operation times of 10 to 100 ns. This now gives the hope for obtaining a stable artificial atom without revolutionizing the conventional junction fabrication technique. By removing bias-lines and exposing the qubit to minimal microwave radiations, these experiments can be indicative of how coherent an Al/AlO_x/Al junction can be.[11–13] What we have learned from these experiments is that we may have to re-examine what we have done in the past, and really master the circuit engineering technique to maximally isolate the qubit from its environment, while maintaining enough tunability for gate operations.

Along with the improvement in qubit coherence, great efforts have also been devoted to the development of the readout technology. From the repetitive to the single-shot measurement, the qubit readout efficiency and speed have both been improved steadily over the last several years. Furthermore with the introduction of the ultra-low noise amplifier that works at the quantum limit,[21] the powerful single-shot quantum non-demolition (QND) readout now be-

*Project supported by the National Basic Research Program of China (Grant No. 2012CB927404), the National Natural Science Foundation of China (Grant Nos. 11222437 and 11174248), the Natural Science Foundation of Zhejiang Province, China (Grant No. LR12A04001), the Program for New Century Excellent Talents in University of Ministry of Education of China (Grant No. NCET-11-0456), and the Synergetic Innovation Center of Quantum Information and Quantum Physics.

†Corresponding author. E-mail: hhwang@zju.edu.cn
‡Corresponding author. E-mail: ychen@physics.ucsb.edu

© 2013 Chinese Physical Society and IOP Publishing Ltd

comes available,[22] which is fast enough to deliver the realtime, meausuement-based quantum feedback control of the qubit.[23,24] This demonstration presents a crucial step towards fault-tolerant quantum computation.

Here, we review recent progress in the coherence and readout of superconducting qubits (For more comprehensive reviews on superconducting qubits, see Refs. [16], [25], [26], [27], and [28]). We begin with introducing some basic concepts in Josephson junctions and superconducting qubits. We then discuss how qubit coherence has been improved, with a focus on the three energy loss mechanisms: dissipation due to external circuitry, TLS defects, and quasiparticle tunneling. We finish by reviewing the progress in the qubit readout, particularly highlighting achievements in the fast QND measurement.

2. Basic concepts

2.1. Josephson junction basics

A Josephson junction consists of two superconducting electrodes separated by a thin insulating barrier, as illustrated in Fig. 1(a). The thin-film superconducting electrodes, typically of Al, Nb, or Re, are sputtered or ebeam-evaporated with a pre-growth vacuum as high as 10^{-10} Torr (1 Torr = 1.33322×10^2 Pa). The insulating barriers are usually native oxide, grown *in situ* by thermal oxidation in pure oxygen. There have been experimental efforts of growing crystalline oxide in a trilayer structure.[29,30] But the best junctions, built on which the qubits have good coherence performance, are grown using double-angle evaporation and *in situ* thermal oxidation in an ultra-high vacuum ebeam evaporator.[11,20]

As a consequence of its sandwich geometry, the junction has a self-capacitance $C_J = \varepsilon_r\varepsilon_0 A/t$, where A is the junction area, t ($\sim$ 1 to 2 nm) is the insulating-barrier thickness, and ε_r is the relative permittivity of the insulating barrier (for AlO_x, $\varepsilon_r \approx 10$). Depending on the junction size, C_J varies from ~ 0.1 fF to ~ 1 pF, C_J directly determines the charging energy $E_C = e^2/(2C_J)$ of the junction.

Another important parameter for a Josephson junction is its critical current I_0, the maximum supercurrent that the junction can support. The actual supercurrent through the junction is related to the phase δ across the Josephson junction through the DC Josephson relation, $I = I_0 \sin\delta$. For a junction in a closed loop ignoring the geometric inductance, δ is related to the flux threading the loop by $\delta = 2\pi\Phi/\Phi_0$, where Φ_0 is the flux quantum. The effective inductance L_J of the Josephson junction is therefore

$$L_J = \frac{d\Phi}{dI} = \frac{\Phi_0}{2\pi I_0 \cos\delta} = \frac{L_{J0}}{\sqrt{1-(I/I_0)^2}}, \qquad (1)$$

where $L_{J0} = \Phi_0/(2\pi I_0)$. The junction inductance L_J is nonlinear and can be tuned with a bias current, enabling the frequency tunability of superconducting qubits. From the DC and AC Josephson relations, the junction energy is $U = -E_J\cos(\delta)$, where $E_J = I_0\Phi_0/(2\pi)$. Therefore, I_0 determines both junction's zero-bias inductance L_{J0} and the Josephson energy E_J.

Thus one can quote the two pairs of parameters to characterize a Josephson junction, either (L_{J0}, C_J) or (E_J, E_C). A Josephson junction is essentially a nonlinear LC resonator, with L_J tuned by a bias current, as illustrated in Fig. 1(b). The pair of parameter (E_J, E_C) will be useful when discussing the potential-well landscapes of the three basic types of qubits.[25]

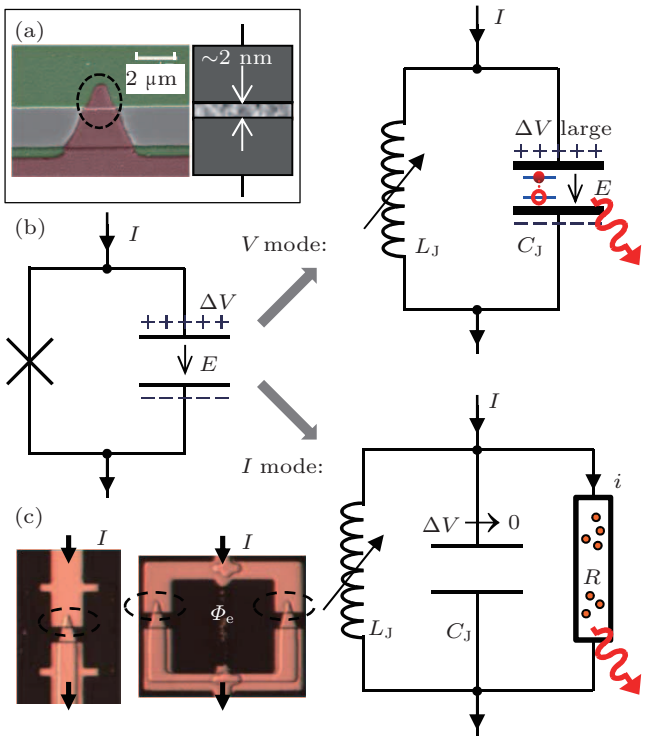


Fig. 1. Josephson junction and its two operation modes. (a) Left: False color scanning electron microscopy image of a phase qubit junction, with top electrode circled at the triangle tip. Insulating barrier is formed by oxidizing the surface of the bottom electrode underneath the triangle tip. Right: Cross-section illustration showing the 2-nm-thick oxide barrier. (b) A Josephson junction can be described as a nonlinear inductor L_J in parallel with its self-capacitance C_J. Depending on whether voltage builds up across C_J, two operation modes related to energy loss can be identified. In the voltage mode, the oscillating voltage builds up across C_J, with the stored electric field (E) energy close to one energy quantum. Oscillating E-field can drive spurious TLS defects (see text) in the insulating barrier, resulting in energy loss. This mode applies to charge and phase qubits. In the current mode, the voltage drop across C_J is minimal and the Josephson junction carries a total current I. TLS loss is negligible but loss from quasiparticle tunneling ($\propto i^2$, where i, the current that flows through the dissipative channel, is a portion of I.) may become serious. This mode applies to the flux qubit, phase qubit, fluxonium,[31] and the 2-junction SQUID (see (c)) for tuning the coplanar waveguide resonator.[32–34] Engineering a circuit incorporating a Josephson junction can mix these two modes to reduce energy loss (see text). (c) Optical micrograph of a single junction (left) and a 2-junction SQUID (right). The 2-junction SQUID can be treated as a single junction with the Josephson energy E_J tuned by an external flux Φ_e, and is used to replace the single junction if tunability is desired. However, this sacrifices coherence due to noise associated with Φ_e.

As a Josephson junction is at the heart of a qubit circuit, it might be helpful to first examine decoherence sources associated with the junction itself. One decoherence source is fluctuations of the junction parameters such as I_0 and C_J, which determine the qubit energy (see e.g., Ref. [35]). These fluctuations are usually low frequency noises, and therefore their impact can be minimized efficiently through dynamical decoupling.[36] Here we focus on energy loss mechanisms in the junction. We define two operation modes that relate to two important energy-loss processes as illustrated in Fig. 1(b). The two modes are determined by the amount of voltage built up across C_J. In the voltage mode, there is enough voltage across C_J such that the electrical field (E) energy stored is close to one energy quantum. In the current mode, there is minimal voltage across C_J, so the junction stores most of the magnetic flux energy by carrying high current. The voltage mode is more sensitive to the loss from two-level state (TLS) defects (see below). The current mode is more sensitive to the loss from quasiparticle tunneling (see below). Useful circuit designs usually mix these two modes to minimize energy loss, with the voltage across C_J reduced by a shunting capacitor and the current through the junction reduced by a shunting inductor.

For a single junction, L_{J0} and E_J are pre-defined during device fabrication. A 2-junction superconducting quantum interference device (SQUID) (shown in Fig. 1(c)) or more complex loop of junctions can be treated as a single junction with L_{J0} and E_J tuned by varying the flux Φ_e. It adds flexibility to the circuit design but also introduces extra flux noise from Φ_e.

2.2. Superconducting qubit basics

Superconducting qubits are made by wiring Josephson junctions to circuit elements such as inductor coils and capacitors. For a quantum circuit to be used as a qubit, the circuit Hamiltonian must have solutions with unequally-spaced energy levels. Ratios between E_J and E_C result in three basic types of superconducting qubits: charge, flux, and phase qubit.[25,26] Here we briefly introduce the three types of qubits in Fig. 2. There are variants, such as the quantronium,[6] transmon,[38] fluxonium,[31] and hybrid qubit[39] for improved coherence. But they operate in similar manners.

2.3. Coherence caliber and some notes on dephasing

We quote two characteristic times to quantify coherence performance. The first is the energy relaxation time (lifetime) T_1, the time for a qubit to relax from its excited state $|1\rangle$ to the ground state $|0\rangle$. After energy relaxation for a time τ, an initial pure state $\alpha|0\rangle + \beta|1\rangle$ becomes a probabilistic mixture of the state $\alpha|0\rangle + e^{-\tau/(2T_1)}\beta|1\rangle$ and the state $\sqrt{1-e^{-\tau/T_1}}\beta|0\rangle$, where the squared norm equals the state probability. Microscopically, energy stored in the qubit is dissipated into the environment through various energy exchange processes. In the next section we will discuss two such modes (TLS defects and quasiparticles) and the corresponding energy exchange processes.

The second one quantifies the phase randomization process between the qubit's $|0\rangle$ and $|1\rangle$ states, and is characterized by the dephasing time T_2. T_2 has a contribution from T_1 as energy relaxation naturally reduces probability in $|1\rangle$ and consequently the phase coherence between $|0\rangle$ and $|1\rangle$. Excluding T_1's contribution to T_2, we define a pure dephasing time T_ϕ. Under the influence of the simplest Markovian noise, $1/T_2 = 1/(2T_1) + 1/T_\phi$.[40] Dephasing occurs when a noise source shifts the qubit energy E_{01} over time. All known dominant dephasing sources, such as critical-current noise, charge noise, and flux noise, have been observed to have a $1/f^\alpha$ noise spectrum (i.e., the spectral density of the noise at low frequency f scales as $1/f^\alpha$), where α is close to 1.[35]

For superconducting qubits, dephasing is likely introduced by control or readout signal lines (see yellow regions in Fig. 2). In particular, native surface spin fluctuators on the bias-lines that are integrated close to the qubit may play a dominant role.[35] In transmon and flux qubits, dephasing noise is negligible ($T_2 \approx 2T_1$) at the "sweet spot" defined in Fig. 2.[6,41,42] In phase qubit increasing the shunt inductance is also seen to reduce noise current driven by noise in the flux-bias line, thus increasing T_2.[43] In the 3D cavity protected transmon qubits, where there is no bias-line, T_2 is likely limited by thermal fluctuations of the number of photons confined in the cavity through the qubit-photon dispersive coupling.[11,12] Better thermal anchoring of the 3D cavity can quench the cavity photon fluctuations and thus improve T_2.[12]

As most observed dephasing noises are low-frequency $1/f$ noises, dynamical decoupling[36] sufficiently suppresses dephasing noise and enhances T_ϕ. Moreover, preliminary quantum error correction has been demonstrated to eliminate artificially introduced dephasing noise.[44] As such, it may be less challenging to handle dephasing, particularly if we remove part of the control lines as done in the 3D cavity protected transmon qubit, or reduce the bias-line coupling to qubit. This is at the cost of controllability. But a proper balance may eventually benefit the overall device performance. Therefore next we will only focus on dissipation issues in superconducting qubits.

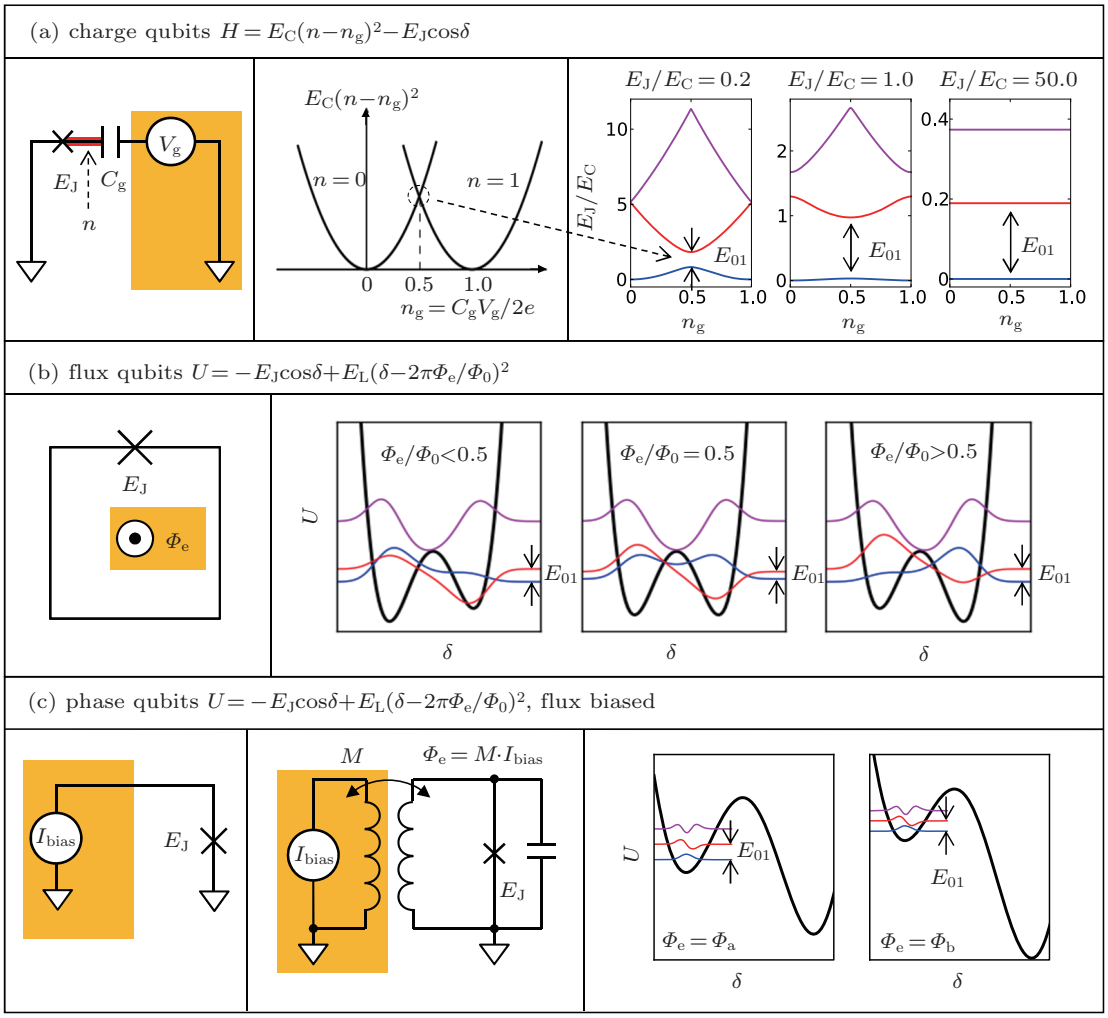


Fig. 2. Introduction to charge, flux and phase qubits.[25,26] Shown are the circuit schematics, potential-well landscapes, eigenenergies, and eigenstate wavefunctions. Yellow regions in schematics denote possible noise sources from external circuitry. (a) Charge qubits.[5] Left: A single junction is gated by an external voltage source V_g. Middle: Charging energy as a function of n_g, where n is the number of Cooper pairs on the island (the red segment in schematic) between the junction and C_g and n_g is the number of Cooper pairs introduced through gating of V_g. The charge qubit is operated at $n_g \approx 0.5$. Right: Normalized eigenenergies E/E_J as functions of n_g at three E_J/E_C values. The lowest three energy levels are indicated by blue, red, and magenta lines, respectively. For $E_J/E_C \ll 1$, the lowest two levels are $(|n=0\rangle+|n=1\rangle)/\sqrt{2}$ and $(|n=0\rangle-|n=1\rangle)/\sqrt{2}$. Qubit energy E_{01} is tuned by n_g, and $\mathrm{d}E_{01}/\mathrm{d}n_g=0$ at $n_g=0.5$. Therefore $n_g=0.5$ is the "sweet spot" for operating a charge qubit. For $E_J/E_C \gg 1$, charges are delocalized and eigenstates are superpositions of different $|n\rangle$, written as $\sum_n c_n|n\rangle$. The ratio E_J/E_C is increased by shunting the junction with an extra capacitor. This produces a transmon qubit, with E_{01} insensitive to fluctuations in n_g away from $n_g=0.5$. (b) Flux qubits.[9,37] Left: Schematic showing a single-junction loop tuned by an external flux Φ_e. Right: Potential-well landscapes (U) as functions of the phase δ across the Josephson junction at three representative Φ_e values. Eigenstate wavefunctions versus δ of the three lowest energy levels are illustrated by the blue, red, and magenta lines, respectively. Qubit energy E_{01} is tuned by Φ_e, and $\mathrm{d}E_{01}/\mathrm{d}\Phi_e=0$ at $\Phi_e/\Phi_0=0.5$. Therefore, $\Phi_e/\Phi_0=0.5$ is the "sweet spot" for operating a flux qubit. (c) Phase qubits.[7,8] Schemaitics of a current-biased single junction (Left) and of a flux-biased single junction (Middle). Right: Potential-well landscapes (U) as functions of the phase δ across the Josephson junction at two Φ_e values ($\Phi_a<\Phi_b$) for the flux-biased single junction. Eigenenergies and wavefunctions of the three lowest energy levels in the left-hand well are illustrated. Qubit energy E_{01} is tuned by Φ_e. There is no "sweet spot" but the phase qubit is less sensitive to noise from Φ_e if operated in a deeper left-hand well.

3. Dissipation in superconducting qubits

3.1. Dissipative environment due to external circuitry

Dissipative environment due to external circuitry, including classical control and measurement instrumentation, might be manageable through dedicated circuit engineering. The interaction between qubit and external circuitry contains two folds of meanings. On one hand, in order to manipulate and measure the qubit, it is necessary to have signal wires that carry electrical signal from the outside instruments to the vicinity of the qubit. On the other hand, the same wires inevitably introduce unwanted noise and a leakage of quantum information from the qubit to the classical environment. An important task is to design a proper intermediate stage between the signal lines and the qubit that can transmit signals while providing the isolation of the qubit from external noise.

Using a flux coil to bias instead of using a current source to directly current-bias the phase qubit junction is one of the examples (see the two schematics in the phase qubit section

in Fig. 2). Coax cables that carry fast DC pulses are 50-Ω-matched, which can be a source of strong dissipation if directly connected to the qubit. Instead, one can use a flux coil that introduces a flux into the qubit loop and generates a circulation current to bias the Josephson junction. The cost is that we need as much as 1-mA current in the flux coil for 1-μA induced current in the qubit loop. Isolation was also done for the readout line of the phase qubit,[45] where dissipation through the readout SQUID back-action may be minimized through the choice of a "sweet spot" (see Fig. 3(a)), similar to those used in charge and flux qubits.[6,41,46] Coupling between the qubit and its readout SQUID can be modeled by a current-to-current transformer, which can be used to calculate the impedance transformation function and to predict the qubit's lifetime T_1. Choosing a proper operation point for minimal transfer of noise is important for achieving a longer T_1, as seen in the right panel in Fig 3(a).

Another example is the use of the Purcell filter to short out the 50-Ω environment, as demonstrated in the transmon qubit[47](see Fig. 3(b)). To ensure the fidelity of the readout, it is critical that all the information stored in the readout cavity can be efficiently transferred to signal acquisition instruments. It therefore requires a large capacitor connecting the readout cavity to external transmission line wiring. However, the strong coupling will at the same time cause the energy dissipation of the qubit, through the Purcell effect.[48] To overcome this problem, a purely reactive $\lambda/4$ resonator is added to modify the environmental admittance at a designed frequency, at which the 50-Ω dissipation channel is shorted out due to a shunted reactive path. The transmon qubit is therefore protected when operated near the frequency of the $\lambda/4$ resonator, but for readout, it will be moved close to the frequency of the readout cavity.

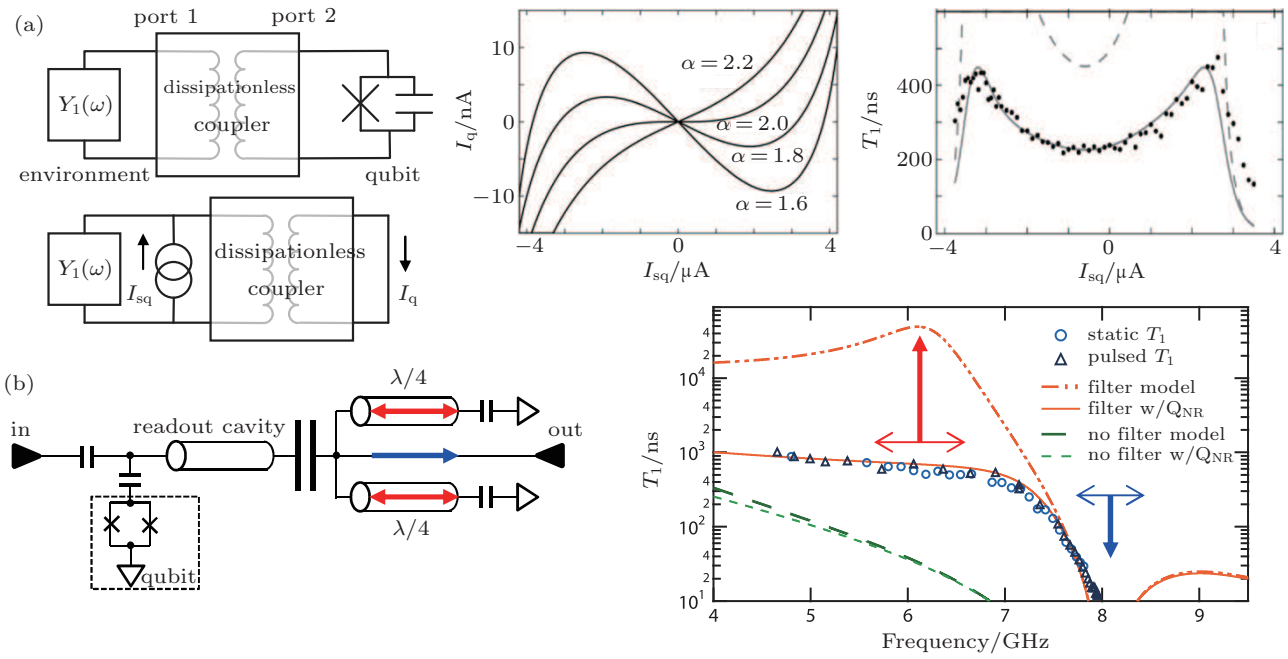


Fig. 3. Examples of decoupling the dissipative external circuitry. (a) Minimizing the readout SQUID's back-action to phase qubit through impedance transformation. Left: Illustrations of impedance transformation by a two-port dissipationless coupler. The external circuitry (environment) dissipation is described by admittance $Y_1(\omega)$. In phase qubits such dissipation comes from the readout SQUID, which is shunted by a 30-Ω resistor to minimize the quasiparticle generation during SQUID's switching. The SQUID inductively couples to the qubit. Admittance $Y_2(\omega)$ (not shown) seen by the qubit is related to $Y_1(\omega)$ through $\mathrm{Re}Y_2(\omega) = \left|\mathrm{d}I_q/\mathrm{d}I_{sq}\right|^2 \mathrm{Re}Y_1(\omega)$, where I_{sq} is the constant biasing current in SQUID during qubit operation and I_q is the I_{sq}-induced current in qubit. For $\mathrm{Re}Y_2(\omega)$ to be small, $\mathrm{d}I_q/\mathrm{d}I_{sq}$ must be as small as possible. Middle: the designed transfer function of I_q versus I_{sq}, which shows that $\mathrm{d}I_q/\mathrm{d}I_{sq} = 0$ at two I_{sq} values for $\alpha < 2$, α is the size ratio between junctions used in the readout SQUID and is designed to be 1.6 in phase qubit. Right: T_1 versus I_{sq} data (dots) measured in a phase qubit. At the two I_{sq} values where $\mathrm{d}I_q/\mathrm{d}I_{sq} = 0$, the qubit shows the longest T_1 values. Line is a fit according to the impedance transformation model. (Panel adapted from Ref. [45]). (b) The Purcell filter to suppress spontaneous emission at the qubit operation frequency. Left: Circuit model of the Purcell-filtered cavity design. The transmon qubit, enclosed in the dash-line box, dispersively interacts with the readout cavity, which strongly couples to external circuitry through C_{out}, C_{out} is designed to be 75 fF, and can lead to unwanted energy loss (through the path indicated by a blue arrow) over a wide range of frequencies. The Purcell filter, implemented with the $\lambda/4$ open-circuited transmission-line stubs, shunts the blue arrow path with high non-dissipative admittance at its resonance frequency ω_r. As such, microwave photons will bounce into the $\lambda/4$ transmission-line stubs (through the path indicated by red arrows) instead of leaking out through the blue arrow path, inhibiting qubit decay near ω_r. Right: Experimental data indicating a region around 8 GHz (resonance frequency of the readout cavity) with very low T_1 values and a region around 6 GHz (resonance frequency of the Purcell filter) with much-improved T_1 performance (Panel modified, with permission, from Ref. [47]).

Although there are many sophisticated designs to isolate noise from the qubit, it is not a simple question to determine how good the isolation should be. Actually, completely removing the dissipation from external circuitry is a real engineering challenge. In a recent experiment, a two-stage transformer is used for a charge qubit. By inserting a lumped-element LC resonator as the intermediate stage, the charge qubit can be effectively decoupled from the transmission line, resulting in a T_1 as high as 200 μs,[10] a 20 times improvement compared with previous results. In other experiments using a 2D[13] or 3D[11,12] cavity protection, the transmon qubits are exposed to minimal microwave radiation, with no bias-line integrated. Although less controllable, these qubits can achieve very long T_1 values close to 100 μs. These long T_1 values suggest that we have to be very careful in dealing with dissipation due to external circuitry.

An inseparable topic associated with the external circuitry is how much dephasing noise it can introduce. The qubits in a 3D cavity without the bias-line have demonstrated good T_2 performance, once the 3D cavity is sufficiently cooled.[12] Similarily, transmon qubits shunted by a capacitor made of TiN and protected in a 2D cavity have also exhibited excellent coherence performance.[13] In contrast, introduction of an integrated bias-line slightly enhanced the dephasing rate.[20] The dephasing noise is possibly associated with the surface spin fluctuators on the bias-line, and may impose a serious materials challenge (a topic not covered by this paper). As mentioned before, by reducing the bias-line coupling to the qubit and performing dynamical decoupling sequences, dephasing noise can be significantly reduced.

There are more aspects to be considered for reducing energy loss by circuit engineering. Radiation loss[49] is one of them but its effect should be small as the circuit is enclosed in a RF tight box. Although all measures add difficulties in circuit fabrication and operation, they do modify the qubit's electromagnetic environment to make the qubit more stable, and are therefore necessary.

3.2. Spurious two-level state defects

Spurious two-level state (TLS) defects are believed to be one important source of energy dissipation.[17] These defects are located inside dielectric layers or surface oxide layers as shown in Fig. 4(a). While the exact microscopic origin of the TLS defects remains unknown, we can model these TLS defects as atomic-scale defects which reside in a double-well potential landscape with two local minima (defined as states $|L\rangle$ and $|R\rangle$).[35] The two local minima differ by energy Δ, and a tunneling path between the two exists (see in Fig. 4(a)). The Hamiltonian for the TLS is

$$H_{\rm TLS} = \frac{1}{2}\begin{pmatrix} \Delta & \Delta_0 \\ \Delta_0 & -\Delta \end{pmatrix}, \qquad (2)$$

where Δ_0 is the tunneling matrix element. In the standard TLS tunneling model Δ is assumed to have a constant distribution and Δ_0 has a distribution $\propto 1/\Delta_0$. The two eigenstates are separated by energy $\varepsilon = \sqrt{\Delta^2 + \Delta_0^2}$.

It has been widely believed that these TLS defects are associated with dangling chemical bonds between atoms. The spatial configuration of bonding electrons between atoms enable an electrical dipole moment $\boldsymbol{d}$ which can resonate with the surrounding electromagnetic field. The interaction between the dipole moment and external electrical field depends on the dipole alignment with the field, $H_{\rm int} = -\boldsymbol{d}\cdot\boldsymbol{E}$. For such an energy exchange process to be effective, the resonant electromagnetic field has to be sufficiently large. In the early designs for charge and phase qubits, there is no shunting capacitor and the Josephson junction itself contains most the electrical energy when fully charged. The electrical field is therefore large enough that the ensemble bath of the TLS defects can absorb the qubit energy and subsquently dissipate it through e.g., phonon radiations.

There have been abundant experimental results which demonstrate the existence of TLS defects.[17,50–55] Due to their spatial arrangement or specific locations in the barrier, some TLS defects can have strong couplings to the qubit and are thus easily observable. The first piece of evidence came from the spectroscopically-resolved spurious two-level systems interacting with the qubit, resulting in avoided two-level crossings (splittings) in the frequency-domain spectroscopy[53] (see an example in Fig. 4(c)). Early evidence of dissipation due to spurious TLS defects was mostly found in phase qubits,[56,57] likely due to the fact that charge and flux qubits use small-size junctions and strongly coupled TLS defects can therefore be statisitcaly avoided. The avoided two-level crossings indicate that other unknown two-level systems are interacting with the qubit when the qubit frequency is close. Their appearance in the frequency domain is random and may drift overtime, in particular after thermal cycles. The complete randomness can be well understood by the conventional dielectric loss model in the low-power limit of single photon, as first systematically formulated for superconducting qubits in the seminal work by Martinis *et al.*[17] In their work, the size distributions of the avoided two-level crossings were statistically studied for phase qubits with junction areas 13 μm^2 and 70 μm^2. The important finding is that there is a significant low-power dielectric loss associated with the insulating barrier of the Josephson junction, an important loss mechanism that had been overlooked for a long time. The model also predicted that a smaller junction is a better choice for statistically avoiding the loss from TLS defects, which was later verified in phase qubits made of smaller-size junctions.[58]

It turned out that the time-domain swap spectroscopy[59] can be used as a powerful tool to locate the strongly cou-

pled TLS defects (see Fig. 4(d)). As illustrated in Fig. 4(b), some TLS defects, usually referred as coherent, can swap energy with the qubit, resulting in Rabi oscillations. In contrast, incoherent TLS defects can quickly dump energy to the surrounding lattice through phonon radiations, acting like a blackhole for absorbing qubit's energy (see an example indicated by the black arrow in Fig. 4(d)). In a recent experiment a systematic study of the strongly coupled coherent TLS was carried out in phase qubits,[60] which measured a distribution of lifetimes of individual TLS defects that can be explained by the standard TLS model. In the experiment they found that the TLS lifetime $T_1 \propto S^{\alpha}$, where $\alpha \approx -1.44$ and S is the coupling strength between the qubit and the TLS defect (the same as the splitting size defined in Fig. 4(c) inset). This is in reasonable agreement with what is expected from the phonon radiation of a dipole (proportional to the coupling strength) inside the junction (a numerical simulation gives $\alpha = -1.63$).

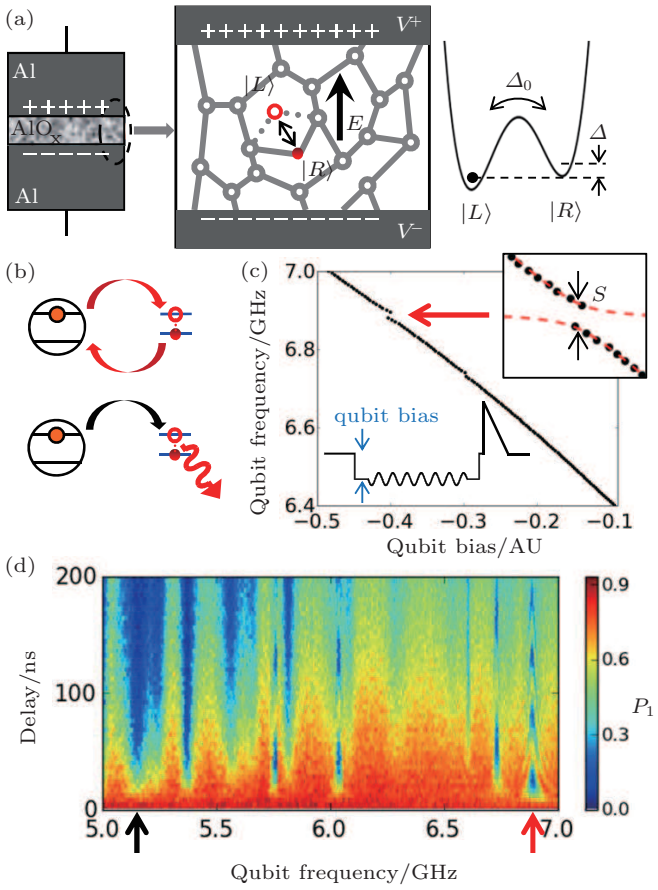


Fig. 4. TLS defects in Josephson junction qubits. (a) Left: Cross-section illustration of a Josephson junction. Middle: TLS defects are located inside the oxide barrier, and are likely related to microscopic charge defects which have two spatial arrangements $|L\rangle$ and $|R\rangle$. Right: In the potential-well description the two local minima are separated by an energy Δ, with a tunneling matrix element Δ_0. (b) Top: A coherent TLS defect can keep energy for a long time. A qubit can exchange energy with it if their frequencies match, resulting in Rabi oscillation between the two. Bottom: An incoherent TLS defect quickly dissipates energy received from qubit to the environment. The two types of TLS defects give very different features in the time-domain swap spectroscopy in ***d***. (c) Frequency-domain qubit spectroscopy. Shown is the qubit resonance frequency as a function of qubit bias. An avoided two-level crossing (splitting), indicated by the red arrow, suggests that a TLS defect interacts with the qubit at about 6.9 GHz. The splitting size S (inset) gives the coupling strength between the qubit and the TLS defect. Inset is the measurement pulse sequence. The measurement starts with biasing the qubit to a certain frequency using the square pulse, followed by a 1-μs-long sinusoidal microwave drive at a selected frequency. Then the qubit excited-state probability P_1 is measured with a triangle pulse. Microwave drive frequency corresponding to maximum in P_1 is recorded as the qubit frequency. (d) Time-domain qubit swap spectroscopy. Shown is the qubit $|1\rangle$-state probability P_1 (colorbar) as a function of qubit frequency (x axis) and delay (y axis). The measurement starts with exciting the qubit to its $|1\rangle$ state, followed by biasing the qubit to a fixed frequency for a delay time. Then qubit P_1 is measured. As indicated by a red arrow at about 6.9 GHz, the qubit swaps its energy into and out of a coherent TLS defect, resulting in P_1 oscillation along the delay axis. This TLS defect is the same as that observed in ***c***. As indicated by a black arrow at about 5.1 GHz, P_1 quickly decays in about 30 ns, suggesting that an incoherent TLS defect may exist.

There are two directions to minimize the TLS loss. As will be discussed later, the efficient method requires the combination of the two. The first one is to use circuit-integrable low-loss dielectric materials, replacing the native oxide dielectrics currently used for Josephson junctions. The TLS model predicts that TLS loss has a strong effect only at very low power close to the single-photon level, and at high powers all TLS defects are saturated with no contribution to energy loss. The simplest way of testing the material loss is to measure the microwave response of an LC resonator with the tested material used as the capacitor dielectrics (see inset of Fig. 5(a)). There have been experimental efforts in search of low-loss dielectric materials at very low powers.[17,29,35,61] SiO_2, the standard dielectric for silicon-based microfabrication, was shown to be particularly lossy at the single-photon level, as compared with the less-lossy ones such as plasma-enhanced-chemical-vapor-deposition (PECVD) grown SiN_x and amorphous Si. Crystalline Si, with highly ordered structure, shows improved performance. Recently, a crystalline sapphire dielectric whispering gallery mode resonator was measured, with the loss tangent of the material to be less than 2×10^{-8} at around 13 GHz.[62] If this crystalline sapphire can be integrated, the upper bound of the qubit T_1 due to the dielectric loss can be up to a millisecond.

However, it is technically very challenging to replace the native oxide with the new dielectrics in the Joshphson junction fabrication process. Great efforts have been invested for epitaxially growing the thin crystalline sapphire layer for the Re/Sapphire/Al hybrid junction.[29,30] However, satisfying results have not been achieved so far. Until today, the Josephson junction with the best performance is still made through the old technique of the double-angle evaporation.

With the junction itself remaining untouched, we can shunt the junction with an extra capacitor using the low-loss dielectrics. With most of the electric field energy stored in the shunting capacitor, we have a minimal amount of the E-field in the Josephson junction barrier, greatly reducing the coupling strength between the qubit and TLS defects. Replacing

the dielectrics with these low-loss materials has directly led to the improvement of phase qubit T_1. From the initial choice of SiN_x to amorphous Si,[17,45,63] and to the more recent crystalline Si,[64] T_1 of phase qubits has risen from 10 ns to more than 1 μs, representing a big understanding of the materials origin. Even though the discovery was made in phase qubits, we believe that this mechanism may also contribute, at least partially, to the improvement of T_1 of transmon qubits over charge qubits,[65] given the fact that vacuum is the lowest-loss dielectric. Recently, hybrid qubits developed by shunting flux qubit junctions with interdigitated capacitors also show coherence time more than 1 μs.[39]

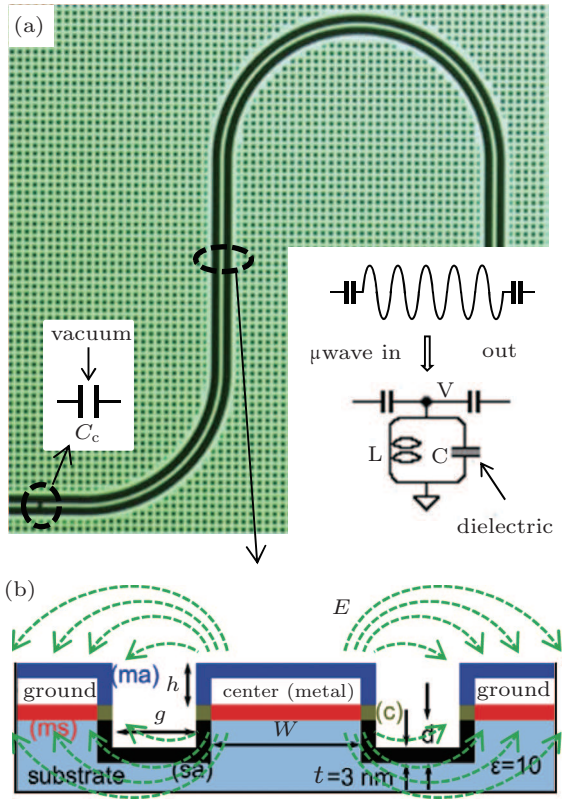


Fig. 5. Understanding TLS dissipation by studying the resonator. Resonators are a simple but efficient platform to test decoherence. (a) Optical micrograph of part of the coplanar waveguide resonator (CPW), with a 5-μm-wide center signal trace and 10-μm gap to the ground plane metallization on either side of the center trace. Green regions are metallization and dark regions are clear with sapphire substrate underneath. The center signal trace is 8-mm-long (half-wavelength) with breaks on both ends (only one end is shown) to support electromagnetic standing waves. The breaks act as vacuum-gap capacitors to couple the resonator to external circuitry (left inset). Right inset: Schematic of the CPW circuit and its equivalent LC circuit to measure the resonator quality factor (Q), which is indicative of sources of dielectric loss in the circuit. For measurement, microwave signals are sent into one port and detected at the other port, which gives the scattering matrix element S_{21} as a function of the microwave frequency. Excitations in the resonator must be close to the single photon energy. There are variants of the circuit but the measurement principles are similar. (b) Cross-section illustration of the CPW highlighting different regions that could contribute to the TLS loss. TLS defects inside these regions could couple with the electric field E (shown as dashed green arrows) when the CPW is excited. These regions include: metal-air (ma) interface, substrate-air (sa) interface, and metal-substrate (ms) interface. Corners are emphasized due to concentrated E-field energies. Geometric scaling analysis and preliminary experiments suggest that overall E-field energy ratio in these regions need to be small for better coherence performance of the circuit (Panel modified, with permissions, from Ref. [67]).

It is important to realize that much of the insight for TLS dissipation comes from the study of resonators. First introduced as kinetic inductance detectors for studying cosmic microwave background radiation, superconducting coplanar waveguide (CPW) resonators are less complicated in structure (Fig. 5(a)) and can easily be scaled up using frequency multiplexing.[66] CPW resonators can also be used to test dielectrics (Fig. 5(a) inset), with the targeted dielectrics either above or below the resonator metal plane, where the electric field E is relatively strong. In the cross-section view of the resonator shown in Fig. 5(b), the metal surface, substrate surface, and the interface between the metal and substrate usually contain layers of oxide or contamination, where TLS defects may reside. In Fig. 5(b) we also illustrate the spatial distribution of the electric field E (indicated by green arrows) when the resonator is charged. As the E-field widely distributes over the space, TLS defects in layers mentioned above can interact with the E-field and thus contribute to energy loss.[40,68,69] Studies show that the energy loss decreases as the resonator trace-width and gap-width become wider, which corresponds to lower surface-to-volume ratios.[40,70] This confirms that the surface layers of the CPW resonator contribute to energy loss. As the E-field focuses at the edge or corner, CPW resonators are also observed to couple with individual TLS defect for coherent energy transfer, similar to the qubit-TLS Rabi oscillation.[34] In a numerical simulation, it is found that the TLS defects in previously overlooked metal-substrate interface may present a dominant dissipation source.[67] Following this idea, CPW resonators fabricated with Al on the pretreated substrate in ultra high vacuum show quality factor above a million,[71] which is a factor of 30 times improvement over previous results. With better choices of superconductors such as TiN_x,[72] it is quite promising that this figure of merit can be further improved.

In resonator studies, the surface oxide, which was originally ignored, is found to contribute significantly to TLS loss. Interdigitated capacitors, mostly relying on vacuum gaps between metallization, were supposed to perform well. However, a series of experiments show that this may not be the case, as a layered oxide or contamination residue may still be present at the metal-air interface.[40,67,68] One of the most significant improvement came with the 3D cavity protected transmon qubit, where the qubit, a Josephson junction with large dipole antenna, is located in the middle of a 3D cavity.[11,12] The 3D cavity has 3-cm^3 mode volume, such that its surface-to-volume ratio is significantly reduced. Later on, other versions of the cavity protected qubits showed up, with an average coherence performance closing to 50 μs.[11–13,20] The Xmon, a 2D cavity protected qubit with bias-line for better controllability, shows up as a promising surface-integrable qubit.[20] 2D cavity protected qubits with shunt capacitors made of TiN_x also show very long coherence.[13]

The route ahead is still possible. With proper circuit engineering, we can avoid the influence of TLS defects, though we cannot control their appearance at the moment. A principle is to always keep an eye on areas in the qubit circuit where the strong E-field can reach.

3.3. Quasiparticles

Another possible source of energy dissipation is nonequilibrium quasiparticles.[18,19,73–76] The incoherent tunneling of quasiparticles across a Josephson junction can lead to dissipation. At temperatures far below the superconducting transition temperature T_c, thermal excitations are suppressed and quasiparticle populations should be negligible. However, unwanted excitations may still be present, possibly due to nonequilibrium sources such as stray infrared radiation, cosmic rays, energy relaxation in materials, or imperfections in qubit control and readout.[18] In flux and phase qubits, the switching of the readout SQUID can dissipate large amounts of energy and generate nonequilibrium quasiparticles. When tunneling across the junction, it is possible for quasiparticles to absorb the qubit energy and subsequently dissipate the energy through phonon radiative loss (see illustrations in Fig. 6(a)). For hot quasiparticles with energies above the superconducting energy gap Δ_{sc}, they may emit photons during tunneling, which can excite the qubit and increase the background $|1\rangle$-state population.[73]

For a small concentration of quasiparticles n_{qp}/n_{cp}, where n_{qp} and n_{cp} are the densities of quasiparticles and Cooper pairs, respectively, the total junction admittance is affected by quasiparticle tunneling as[74]

$$\frac{Y_J(\omega)}{1/R_n} = \frac{\Delta_{sc}}{\hbar\omega}(1+\cos\delta)\left[\frac{1+i}{\sqrt{2}}\sqrt{\frac{\Delta_{sc}}{\hbar\omega}}\frac{n_{qp}}{n_{cp}} - i\pi f(\Delta_{sc})\right] - i\pi\frac{\Delta_{sc}}{\hbar\omega}\cos\delta\,[1-f(\Delta_{sc})], \quad (3)$$

where $f(E=\Delta_{sc})$ describes the occupation probability at Δ_{sc} for nonequilibrium quasiparticles. Here we only consider the low-energy (cold) quasiparticles.

For the Josephson junction phase $\delta = 0$ the factors from $f(\Delta_{sc})$ cancel out, and the admittance is

$$\frac{Y_J(\omega)}{1/R_n} = \sqrt{2}(1+i)\left(\frac{\Delta_{sc}}{\hbar\omega}\right)^{3/2}\frac{n_{qp}}{n_{cp}} - i\pi\frac{\Delta_{sc}}{\hbar\omega}. \quad (4)$$

This formula is equivalent to the normalized conductivity $\sigma(\omega)/\sigma_n$ given by the Mattis–Bardeen theory for thermal quasiparticles in the limit $kT \ll \hbar\omega \ll \Delta_{sc}$, which has been used to describe the effect of quasiparticles on CPW resonators.

There have been systematic studies on the effects of nonequilibrium quasiparticles in phase qubits,[18,74] where the readout SQUID is used as a source to generate nonequilibrium quasiparticles (Fig. 6(b)). In Eq. (3), the real (dissipative) part of the admittance at the qubit frequency, $\mathrm{Re}Y_J(\omega = E_{01}/\hbar)$, increases with increased quasiparticle density n_{qp}/n_{cp}, whereas the imaginary part of Y_J shifts the qubit frequency. In phase qubits, the presence of quasiparticles n_{qp}/n_{cp} also changes the junction's critical current I_0, which directly determines the potential-well landscape and affects, in addition to the effect of $\mathrm{Im}Y_J$, the qubit frequency. Therefore the two quantities, the qubit decay rate $\Gamma_1 = 1/T_1$ and the shift of the qubit frequency $\delta(E_{01}/h)$, can be correlated as they both depend on the quasiparticle density n_{qp}/n_{cp}. Based on the actual parameters of the qubit, $\delta(E_{01}/h)/\Gamma_1$ is theoretically predicted to take values close to -1.0. This was verified experimentally using the repetition rate of the readout SQUID's switching and the switching current magnitudes as knobs to change n_{qp}/n_{cp}. The representative data are shown in Fig. 6(c).[74] A follow-up experiment further reveals the effects of hot nonequilibrium quasiparticles by examining the qubit $|1\rangle$-state probability due to excitations from quasiparticles with energies larger than $E_{01}+\Delta_{sc}$.[73]

One way to reduce the effects of excessive quasiparticles is to engineer quasiparticle traps that can restrict quasiparticles away from the qubit junction and thus forbid the dissipative tunneling from occurring. The quasiparticle traps are typically made of superconductors with an energy gap lower than the regular one: $\Delta_{sc}^{qp} < \Delta_{sc}$. As quasiparticles quickly relax to the gap edge through incoherent phonon scatterings, they have less chance of escaping away from these traps to the nearby regions which are made of superconductors with a regular energy gap Δ_{sc}. In the transmon qubit, the quasiparticle trap was engineered in a reversed way, where clean Al was used for the trap and the Josephson junction was made by oxygen-doped Al. The oxygen-doped Al has an energy gap 280 μeV and T_c 1.9 K, about 60% higher than those of the clean Al (energy gap 180 μeV and T_c 1.2 K).[75] The quasiparticle trap is defined by depositing a layer of clean Al 100 nm away from the junction. The effectiveness of their small-size traps (the quasiparticle diffusion length in Al can be of millimeter lengths,[18] as illustrated in Fig. 6(b)) and the use of oxygen-doped Al for junction electrodes may be questioned. But their findings that quasiparticle-induced relaxation in their system may not be a serious concern for T_1 at the order of 100 μs are encouraging. Small effects of nonequilibrium quasiparticles in the transmon qubit are likely due to the dispersive readout for less energy injection on-chip and the galvanically isolation of qubit junction from the rest circuitry.

Reducing the unwanted excitation sources of quasiparticles is equally important. For flux and phase qubits, large energy dumped on-chip due to the readout SQUID's switching events are serious concerns. A low-energy readout scheme is thus highly necessary, as will be discussed later. Meanwhile, well isolating the devices from the radiative environment using multistage shielding may be a crucial step for completely removing the quasiparticle source.[20]

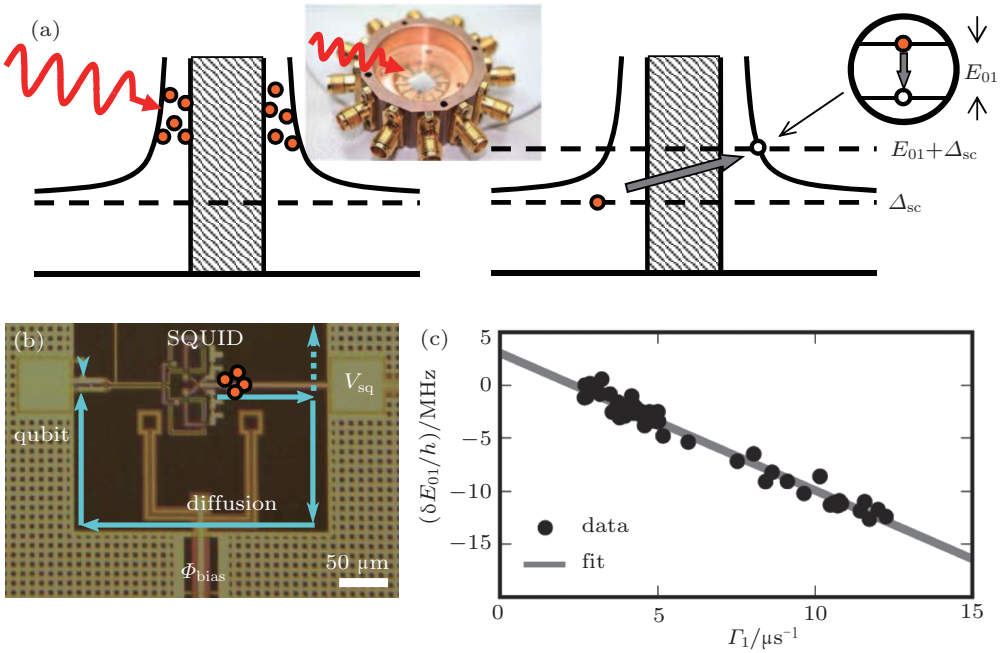


Fig. 6. Dissipation due to quasiparticle tunneling. (a) Illustrations of the dissipation process due to quasiparticle tunneling. Left: Quasiparticles are generated by unwanted irradiation for the sample sealed in the metal box (inset) below 20 mK. The quasiparticles relax to near the superconductor energy gap Δ_{sc} through electron-phonon scattering. Right: During quasiparticle tunneling, there is a probability for a quasiparticle to absorb one energy quantum E_{01} from the qubit, resulting in qubit dissipation. (b) Controlled quasiparticle generation in phase qubit. By switching the readout SQUID to the resistive state with the voltage V_{sq}, quasiparticles can be generated and they eventually diffuse to the nearby qubit junction through path indicated by light blue arrows (Panel adapted from Ref. [73]). (c) Quasiparticle tunneling affects the qubit's dissipation rate Γ_1 as well as the qubit frequency $f = E_{01}/h$. Experiments were carried out in a phase qubit and the frequency shift versus the decay rate is shown, which agrees with theory (Panel adapted from Ref. [74]).

3.4. More about suppressing dissipation

So far we have discussed three energy loss mechanisms. Proper circuit engineering should allow for avoiding most of their influence, but a true breakthrough may rely on the interplay between new materials research and circuit engineering. At the present stage, we are fortunate that, with only a small help from new materials, superconducting qubits have already shown sufficiently long coherence, enough for thousands of coherent operations. The good coherence performance also enables the development of the new readout technique as will be discussed next. A problem for the 3D cavity protected transmon qubits is that they may not be suitable for large-scale integration due to their size and lack of frequency tunability. There are 2D version of the qubits that are tunable in frequency. Although these qubits have slightly reduced coherence performance, foreseeable improvements are next. Meanwhile, all-microwave gates[14,77] have been demonstrated by the IBM group, in which virtual couplings through the resonator cavity were implemented to coupled qubits at fixed frequencies. The operation employs simple amplitude control of a single microwave tone, and qubit biasing is unnecessary. However, the gate time is significantly longer than that in previous demonstrations when qubit biasing is possible.

It is likely that a small capability to bias the qubit may still be necessary. A way out is to have minimal qubit tunability together with the all-microwave gates. The capability of tuning the qubit and even the cavity resonator[34] may prove useful when implementing gate-based operations to protect the qubit against decoherence.

Quantum error correction, capable of correcting error syndromes if detected, has been preliminarily demonstrated in transmon qubits with artificially introduced bit-flip and phase errors.[44] However, the capability of correcting errors due to dissipation is yet to come. Recently there is a proposal of correcting photon-loss errors by encoding/decoding the qubit state using the resonator cavity mode.[78] The method uses the large Hilbert space in the resonator cavity to redundantly encode quantum information, which is different from the QEC code[79] and surface code[80] that use the multiqubit register. Moreover, as an alternative shortcut in certain applications, a probabilistic way to suppress dissipation errors has been demonstrated recently based on the idea of quantum uncollapsing, in which errors are rejected if detected.[81] These algorithm-based quantum control methods represent another powerful tool to suppress the influence of dissipation for quantum information processing.

4. Quantum measurement

4.1. Basic concepts

Together with much improved qubit coherence, there has been rapid progress in the readout technology over the last

decade. The capability to identify the state of qubit is crucial for almost all the protocols in quantum information processing. The three essential requirements for an ideal readout are: (i) High fidelity: the capability of reading out accurately, (ii) High speed: the capability of reading out rapidly, and (iii) Low back-action: the capability of reading out without decohering the qubit. Satisfying these three requirements is in principle very sound. Unfortunately, in practice it is very challenging. These challenges have been the main driving force behind the development of the superconducting qubit readout technology.

For a quantum system, the qubit state is usually directly reflected in the status of a certain quantum variable. A charge qubit, for example, has its quantum states encoded into states with different charge numbers. A flux qubit, on the other hand, has its quantum states associated with states of different flux threading the circuit loop. A natural solution to read out the qubit states would therefore be to use the well-engineered detectors which are ultra-sensitive to those quantum variable signals. This is, in fact, the approach that researchers initially took, when single electron transistors (SETs) were used as charge detectors to read out charge qubits and SQUIDs were used as flux detectors to read out flux and phase qubits.[7,9,82] These approaches have demonstrated good performance in readout fidelity and speed, but are limited by rather strong back-actions in the form of current noise or excessive quasiparticles.

4.2. Dispersive readout: repetitive and single-shot

With the emergence of the circuit quantum electrodynamics (cQED) architecture, researchers developed a new readout technique–dispersive readout, which turned out to be a powerful one applicable to all kinds of superconducting qubits.[83,84] As shown in Fig. 7(a), the principle of the dispersive readout lies in the fact that there is a dispersion-induced resonance frequency shift for a superconducting resonator when being coupled to a qubit. As the resonance frequency shift depends on whether the qubit is in the ground or the excited state, one can read out the qubit state by probing the microwave response of the resonator. In other words, when measuring at a certain frequency, different qubit states will be projected into different transmission (or reflection) coefficients. Expressing the transmission (or reflection) coefficient in forms of a complex number $I + \mathrm{i}Q$, one can find out that the measured signals for a qubit being in the ground state and excited state correspond to two distinct points in the I–Q plane, as shown in Fig. 7(b). Meanwhile, there is noise in the measurement system, which gives rise to random scattering of the signal points in the I–Q plane. Clearly, the success of the readout is mainly determined by the signal-to-noise ratio, i.e., the separation of the two signal points over the size of the scattering blot. The real challenge is to achieve a high signal-to-noise ratio within a short period of measurement time, without adding decoherence to the qubit.

The simplest approach to increase the signal-to-noise ratio is through the repetitive measurements. This was, in fact, the most commonly used method at the early stage of the dispersive readout. In order to achieve a signal-to-noise ratio sufficient to distinguish the two states, one had to repeat the measurement to effectively average out the noise. With an average of about 5×10^4 measurements, it has been demonstrated that one can achieve a readout signal-to-noise ratio as high as 25, enabling the single qubit characterizations such as the Rabi oscillation and the Ramsey fringe measurements.[85]

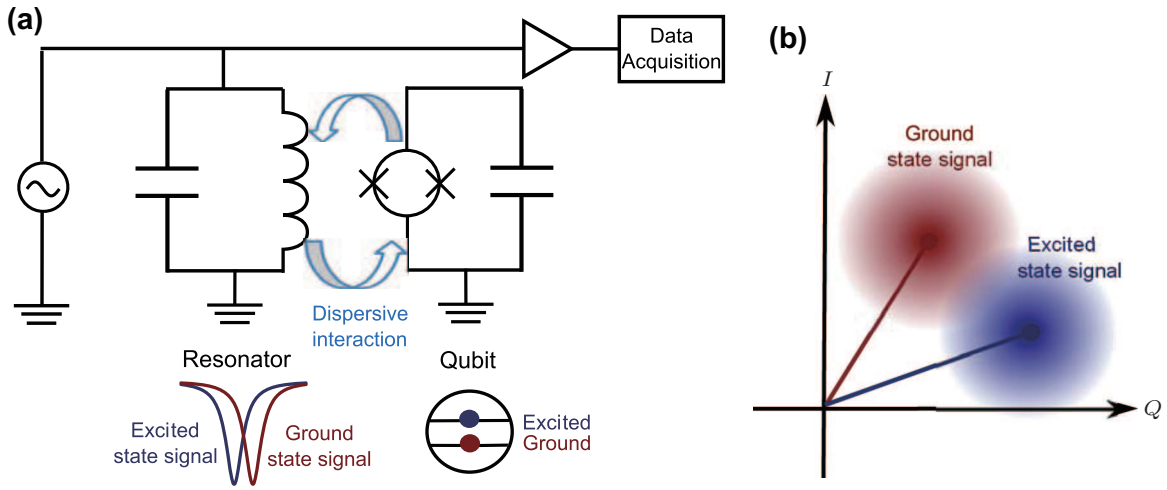


Fig. 7. Dispersive readout. (a) Top: Circuit schematic of dispersive readout showing a resonator coupled to a qubit. Bottom: Illustration of a qubit state-dependent resonator frequency shift due to the dispersive resonator-qubit interaction. (b) When expressed as a complex number $I + \mathrm{i}Q$, the readout signal corresponds to a point in the complex I–Q plane, whose position depends on the state of the qubit. The system noise will induce random distortion of the signal, therefore leading to spreading out of the signal points in the I–Q plane.

Despite the success in reading out single qubit, the repetitive readout met its limit when multiple qubits need to be measured simultaneously. Given the averaged nature, the repetitive readout is unable to resolve the qubit–qubit correlation and therefore forbids the exploration of the multi-qubit dynamics such as entanglement. To solve this issue, people switched from the repetitive dispersive readout to single-shot readout. The fidelity of the single-shot readout, where the qubit state gets evaluated individually during each measurement, is directly determined by the accuracy of identifying the qubit state within the measurement probe time. Similar to the repetitive readout whose fidelity gets improved with increasing number of measurements, one can reduce the single-shot readout noise by increasing the probe time. In practice, however, this approach still has a limited readout fidelity simply due to the energy decay of the qubit.

On the other hand, an improved signal-to-noise ratio can be achieved by enhancing the signal, namely, the separation of the two signal points in the I–Q plane. A naive thought is that one would achieve an enhanced signal by turning up the resonator readout power. There are associated subtleties, unfortunately, when the number of photons in the readout resonator is increased. At the same time that the resonator gets a qubit-state-dependent frequency shift, the qubit frequency also varies with the photon number in the resonator, which is the AC Stark shift. As a consequence, the quantum fluctuation of the photon number (photon shot noise) will directly give rise to random shifting in the qubit frequency and eventually measurement-induced dephasing.[84] However, it turned out that one can achieve an enhanced readout signal if further increasing the resonator readout power. In the strong driven dispersive regime, it has been discovered that there exists an unexpected onset of "Bright state", where the transmission of the microwave abruptly increases, as shown in Figs. 8(a)–8(e).[86] The associated critical power level at the onset of the "Bright state" depends sensitively on the state of the qubit. With a properly chosen readout power, the ground or excited state in the qubit can be projected into the "Dark" or "Bright" state in the resonator, which effectively enhances the signal-to-noise ratio by pulling the readout signal of the excited state further away from that of the ground state. The concept of enhancing the signal through state projection was already used in phase qubits. Given that it is operated in a tilted potential well, the phase qubit can be biased by a short DC measure pulse, which projects its ground state or the excited state into the "Left well" or "Right well" state (see introduction to the phase qubit in Fig. 2). As with the "Dark" and "Bright" states, the "Left well" and "Right well" states yield much higher signal separation compared to that of the bare qubit states.[66] Therefore with an inductively coupled lumped element resonator, one can easily readout the qubit state with high single-shot fidelity, as shown in Figs. 8(f) and 8(g).

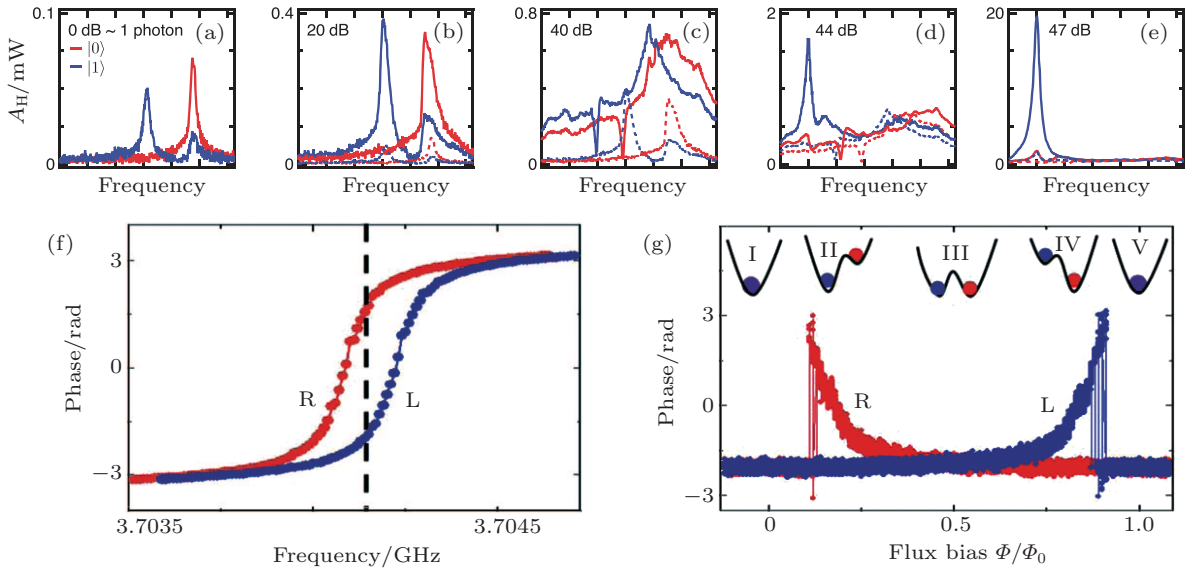


Fig. 8. Single-shot readout through state projection. (a)–(e) The "Bright state" readout: The resonator response as a function of frequency at different drive power levels (the 0 dB here corresponds to single photon). One can see the evolution of the readout signal: at low power, there is a dispersion-induced frequency shift between the ground state and excited state signal. At high power, the frequency shift vanishes, but the amplitude of the readout signal shows drastic difference between the ground state and excited state signal. As seen, 47 dB is the optimal drive power level for differentiating the qubit states (Panels reproduced, with permission, from Ref. [86]). (f) and (g) The "Left well" and "Right well" state readout: The resonator response, after the coupled qubit is projected into the "Left well" (L) and "Right well" (R) states. The projection greatly enhances the readout signal by increasing the dispersive frequency shift between the ground and excited state signals. One can perform multiple signal-shot measurements at different qubit biases and find out that the two readout signals are well separated. A signal-to-noise ratio as high as 10 guarantees the high fidelity of the readout (Panels reproduced, with permission, from Ref. [66]).

Instead of projecting the state of the qubits, one can also achieve an enhanced signal separation by directly projecting the states of the resonator.[87–90] This is realized through exploring the bifurcation regime of the nonlinear resonator. With a single Josephson junction or a SQUID embeded (see Fig. 1(c)), a linear resonator inherits nonlinearity from the nonlinear inductance of the Josephson junction. Over a limited range of driving power, a nonlinear resonator can be tuned into the bifurcation regime, where there coexist two bistable states with dramatically different microwave responses. One can perform a launching process to project the resonator into either states, by adjusting driving power of the resonator. When having the nonlinear resonator coupled to the qubit, the result of the projection actually depends on the state of the qubit. This qubit state-dependent projection is the key to the single-shot readout using a nonlinear resonator.

Unfortunately, the approach of readout through state projection has a two-fold consequence. At the same time that the readout signal is enhanced, the state projection has to pay the price of the reduced readout speed. After reading out the qubit, one has to either reinitialize the qubit (if the qubit is projected), or need to wait for the resonator to fully relax (if the resonator is projected). The delay in readout speed severely affects the efficiency of executing more advanced protocols such as quantum feedback and quantum error correction.

4.3. Quantum-limited superconducting amplifier and single-shot QND readout

After all the efforts of enhancing the readout signal, the real breakthrough of the readout technology eventually came after the success of suppressing the readout noise. The system noise level is to a large extent determined by the noise temperature of the first-stage amplifier in the readout circuit. The basic operation principle of an amplifier is usually based on the sensitive dynamic change of a certain signal (acting as the output signal) in response to the other one (acting as the input signal). It requires the usage of nonlinear elements such as transistors, which are typically dissipative and can add additional noise to the signal. Cryogenic semiconductor high-mobility-electron-transistor (HEMT) amplifiers, for example, have a noise temperature around 3 K–4 K, corresponding to a noise level of tens of photons in contrast to merely a few photons of the signal to be detected. Minimizing the noise temperature therefore requires a dissipationless nonlinear element and fortunately it can be satisfied by the superconducting Josephson junction. Researchers have demonstrated that a nonlinear resonator, which is a 2-junction SQUID loop shunted with a capacitor, can be used as an amplifier when being strongly driven.

The behavior of the nonlinear resonator under an AC drive can be described as

$$C\frac{\Phi_0}{2\pi}\frac{\mathrm{d}^2\delta(t)}{\mathrm{d}t^2}+\frac{1}{Z_0}\frac{\Phi_0}{2\pi}\frac{\mathrm{d}\delta(t)}{\mathrm{d}t}+I_0\sin(\delta(t))=I_\mathrm{d}\cos(\omega_\mathrm{d}t), \quad (5)$$

where C is the shunted capacitance, Z_0 is the real impedance of the circuit, I_0 is the critical current of the SQUID, and I_d is the drive signal amplitude. One can solve such a nonlinear differential equation and find out that a high amplitude drive can drive the system to the bifurcation regime discussed above, where there are three solutions for δ.[91,92] Just below the bifurcation regime, the nonlinear resonator has a single-value but steeper response to the drive signal. In this parametric regime, a small modulation in the resonator drive can result in a large microwave response, exactly the transfer function required for an amplifier. With a persistent effort over the last several years, Josephson parametric amplifiers (JPAs) have been successfully developed based on the nonlinear resonators.[21] Operated in the superconducting state without dissipation, the JPA has demonstrated excellent performance with a noise level limited to half a photon, purely the zero-point fluctuation of the electromagnetic field. With a quantum-limited noise and a high gain over 20 dB, these ultra-low noise amplifiers serve as a perfect preamp for the cryogenic HEMT amplifier and result in dramatic improvement in the readout efficiency. Even with a probe time only a few percent of the qubit coherence time, one can acquire a signal-to-noise ratio which is sufficiently high to ensure the high fidelity for a single-shot readout. What is more crucial, such a high-fidelity single-shot readout is achieved without the hassle of enhancing the resonator readout signal through the state projection. It preserves the eigenstates of the qubit with very low back-actions, qualifying this way of readout as a QND readout.

The success of single-shot QND readout brings profound influence on the progress of superconducting quantum computation. As demonstrated with the first observation of quantum jumps in superconducting qubits, we are now able to perform high-fidelity, real-time monitoring on the state of the qubit.[22] With such a capability, the readout is no longer necessarily the last step to be performed in the whole control sequence, therefore, allowing us to go beyond the current open-loop control scheme to a closed-loop feedback control scheme. In other words, the qubit can now receive realtime instructions, based on the result of monitoring the qubit state. Being able to perform the closed-loop control on the system using quantum feedback represents a major step forward for fault-tolerant superconducting quantum computation. Initial efforts are made to demonstrate the power of the closed-loop control using quantum feedback. Using a weak measurement to monitoring the qubit state, researchers have shown that closed-loop feedback control can be used to overcome dephasing and stabilize

the Rabi oscillation of a qubit indefinitely.[23] More recently, a deterministic qubit initialization protocol has been demonstrated, where the quantum feedback control has been applied to remove the spurious excitation in the qubit.[24,93] Such a high-fidelity quantum feedback control delivered by single-shot QND readout will be a critical component of quantum error correction.

5. Closing remarks

With the long coherence time and high-fidelity QND readout achieved, superconducting qubits are now one-step closer to realizing fault-tolerant quantum computation. We will continue to enjoy the high coherence that the simple Al/AlO_x/Al junction can provide, by refining the circuit design and fabrication process. We believe that the materials research on low-loss dielectrics will eventually become fruitful and may lead to another big leap of the qubit coherence. Meanwhile, further development of the readout technology will continue to focus on enhancing the QND readout fidelity and speed, with a key addition of the multiplexing function for scalability. Despite all the challenges ahead, we are optimistic since there seem to be no fundamental limitations on the future of superconducting qubits.

Acknowledgments

We thank Wenner J and Xu K for valuable discussions.

References

[1] Devoret M H, Martinis J M and Clarke J 1985 *Phys. Rev. Lett.* **55** 1908
[2] Martinis J M, Devoret M H and Clarke J 1985 *Phys. Rev. Lett.* **55** 1543
[3] Leggett A J, *Chance and Matter*, Proceedings of the Les Houches Summer School, Session XLVI, edited by Souletie J, Vannimenus J and Stora R (North-Holland, Amsterdam, 1987), p. 395
[4] Nakamura Y, Chen C D and Tsai J S 1997 *Phys. Rev. Lett.* **79** 2328
[5] Nakamura Y, Pashkin Y A and Tsai J S 1999 *Nature* **398** 786
[6] Vion D, Aassime A, Cottet A, Joyez P, Pothier H, Urbina C, Esteve D and Devoret M H 2002 *Science* **296** 886
[7] Martinis J M, Nam S and Aumentado J 2002 *Phys. Rev. Lett.* **89** 117901
[8] Yu Y, Han S Y, Chu X, Chu S and Wang Z 2002 *Science* **296** 889
[9] Chiorescu I, Nakamura Y, Harmans C J P M and Mooij J E 2003 *Science* **299** 1869
[10] Kim Z, Suri B, Zaretskey V, Novikov S, Osborn K D, Mizel A, Wellstood F C and Palmer B S 2011 *Phys. Rev. Lett.* **106** 120501
[11] Paik H, Schuster D I, Bishop L S, Kirchmair G, Catelani G, Sears A P, Johnson B R, Reagor M J, Frunzio L, Glazman L I, Girvin S M, Devoret M H and Schoelkopf R J 2011 *Phys. Rev. Lett.* **107** 240501
[12] Rigetti C, Gambetta J M, Poletto S, Plourde B L T, Chow J M, C'orcoles A D, Smolin J A, Merkel S T, Rozen J R, Keefe G A, Rothwell M B, Ketchen M B and Steffen M 2012 *Phys. Rev. B* **86** 100506
[13] Chang J B, Vissers M R, Córcoles A D, SandBerg M, Gao J S, Abraham DW, Chow J M, Gambetta J M, RothwellM B, Keefe G A, Steffen M and Pappas D P 2013 *Appl. Phys. Lett.* **103** 012602
[14] Chow J M, Gambetta J M, Córcoles A D, Merkel S T, Smolin J A, Rigetti C, Poletto S, Keefe G A, Rothwell M B, Rozen J R, Ketchen M B and Steffen M 2012 *Phys. Rev. Lett.* **109** 060501
[15] Gustavsson S, Zwier O, Bylander J, Yan F, Yoshihara F, Nakamura Y, Orlando T P and Oliver W D 2013 *Phys. Rev. Lett.* **110** 040502
[16] Devoret M H and Schoelkopf R J 2013 *Science* **339** 1169
[17] Martinis J M, Cooper K B, McDermott R, Steffen M, Markus A, Osborn K D, Cicak K, Oh S, Pappas D P, Simmonds R W and Yu C C 2005 *Phys. Rev. Lett.* **95** 210503
[18] Martinis J M, Ansmann M and Aumentado J 2009 *Phys. Rev. Lett.* **103** 097002
[19] Catelani G, Koch J, Frunzio L, Schoelkopf R J, Devoret M H and Glazman L I 2011 *Phys. Rev. Lett.* **106** 077002
[20] Barends R, Kelly J, Megrant A, Sank D, Jeffrey E, Chen Y, Yin Y, Chiaro B, Mutus J, Neill C, O'Malley P, Roushan P, Wenner J, White T C, Cleland A N and Martinis J M 2013 *Phys. Rev. Lett.* **111** 080502
[21] Hatridge M, Vijay R, Slichter D H, Clarke J and Siddiqi I 2011 *Phys. Rev. B* **83** 134501
[22] Vijay R, Slichter D H and Siddiqi I 2011 *Phys. Rev. Lett.* **106** 110502
[23] Vijay R, Macklin C, Slichter D H, Weber S J, Murch K W, Naik R, Korotkov A N and Siddiqi I 2012 *Nature* **490** 77
[24] Riste, Bultink C C, Lehnert K W and DiCarlo L 2012 *Phys. Rev. Lett.* **109** 240502
[25] You J Q and Nori F 2005 *Phys. Today* **58**(11) 42
[26] Clarke J and Wilhelm F K 2008 *Nature* **453** 1031
[27] You J Q and Nori F 2011 *Nature* **474** 589
[28] Xiang Z L, Ashhab S, You Y J and Nori F 2013 *Rev. Mod. Phys.* **85** 623
[29] Oh S, Cicak K, McDermott R, Cooper K B, Osborn K D, Simmonds RW, Steffen M, Martinis J M and Pappas D P 2005 *Supercond. Sci. Technol.* **18** 1396
[30] Kline J S, Wang H H, Oh S, Martinis J M and Pappas D P 2009 *Supercond. Sci. Technol.* **22** 015004
[31] Manucharyan V E, Koch J, Glazman L I and Devoret M H 2009 *Science* **326** 113
[32] Sandberg M, Wilson C M, Persson F, Bauch T, Johansson G, Shumeiko V, Duty T and Delsing P 2008 *Appl. Phys. Lett.* **92** 203501
[33] Yamamoto T, Inomata K, Watanabe M, Matsuba K, Miyazaki T, Oliver W D, Nakamura Y and Tsai J S 2008 *Appl. Phys. Lett.* **93** 042510
[34] Wang Z L, Zhong Y P, He L J, Wang H, Martinis J M, Cleland A N and Xie Q W 2013 *Appl. Phys. Lett.* **102** 163503
[35] McDermott R 2009 *IEEE Trans. Appl. Supercond.* **19** 2
[36] Bylander J, Gustavsson S, Yan F, Yoshihara F, Harrabi K, Fitch G, Gory D G, Nakamura Y, Tsai J S and Oliver W D 2011 *Nat. Phys.* **7** 565
[37] Friedman J R, Patel V, Chen W, Tolpygo S K and Lukens J E 2000 *Nature* **406** 43
[38] Koch J, Yu T M, Gambetta J, Houck A A, Schuster D I, Majer J, Blais A, Devoret M H, Girvin S M and Schoelkopf R J 2007 *Phys. Rev. A* **76** 042319
[39] Steffen M, Kumar S, DiVincenzo D P, Rozen J R, Keefe G A, Rothwell M B and Ketchen M B 2010 *Phys. Rev. Lett.* **105** 100502
[40] Wang H, Hofheinz M, Ansmann M, Bialczak R C, Lucero E, Neeley M, O'Connell A D, Sank D, Wenner J, Cleland A N and Martinis J M 2009 *Phys. Rev. Lett.* **103** 200404
[41] Yoshihara F, Harrabi K, Niskanen A O, Nakamura Y and Tsai J S 2006 *Phys. Rev. Lett.* **97** 167001
[42] Kakuyanagi K, Meno T, Saito S, Nakano H, Semba K, Takayanagi H, Deppe F and Shnirman A 2007 *Phys. Rev. Lett.* **98** 047004
[43] Sank D, Barends R, Bialczak R C, Chen Y, Kelly J, Lenander M, Lucero E, Mariantoni M, Megrant A, Neeley M, O'Malley P J J, Vainsencher A, Wang H, Wenner J, White T C, Yamamoto T, Yin Y, Cleland A N and Martinis J M 2012 *Phys. Rev. Lett.* **109** 067001
[44] Reed M D, DiCarlo L, Nigg S E, Sun L, Frunzio L, Girvin S M and Schoelkopf R J 2012 *Nature* **482** 382
[45] Neeley M, Ansman M, Bialczak R C, Hofheinz M, Katz N, Lucero E, O'Connell A, Wang H, Cleland A N and Martinis J M 2008 *Phys. Rev. B* **77** 180508
[46] Astafiev O, Pashkin Y A, Nakamura Y, Yamamoto T and Tsai J S 2004 *Phys. Rev. Lett.* **93** 267007
[47] Reed M D, Johnson B R, Houck A A, DiCarlo L, Chow J M, Schuster D I, Fruncio L and Schoelkopf R J 2010 *Appl. Phys. Lett.* **96** 203110
[48] Purcell E M 1946 *Phys. Rev.* **69** 674
[49] Sandberg M, Vissers M R, Ohki T A, Gao J S, Aumentado J, Weides M and Pappas D P 2013 *Appl. Phys. Lett.* **102** 072601
[50] Plourde B L T, Robertson T L, Reichardt P A, Hime T, Linzen S, Wu C and Clarke J 2005 *Phys. Rev. B* **72** 060506
[51] Zaretskey V, Suri B, Novikov S, Wellstood F C and Palmer B S 2013 *Phys. Rev. B* **87** 174522
[52] Ithier G, Collin E, Joyez P, Meeson P J, Vion D, Esteve D, Chiarello F, Shnirman A, Makhlin Y, Schriefl J and Schn G 2005 *Phys. Rev. B* **72** 134519

[53] Simmonds R W, Lang K M, Hite D A, Nam S, Pappas D P and Martinis J M 2004 *Phys. Rev. Lett.* **93** 077003

[54] Tian L and Simmonds R W 2007 *Phys. Rev. Lett.* **99** 137002

[55] Simmonds R W, Allman M S, Altomare F, Cicak K, Osborn K D, Park J A, Sillanpää M, Sirois A, Strong J A and Whittaker J D 2009 *Quantum Inf. Process.* **8** 117

[56] Yu Y, Zhu S L, Sun G Z, Wen X D, Dong N, Cheng J, Wu P H and Han S Y 2008 *Phys. Rev. Lett.* **101** 157001

[57] Sun G Z, Wen X D, Mao B, Chen J, Yu Y, Wu P H and Han S Y 2010 *Nat. Commun.* **1** 51

[58] Lucero E, Barends R, Chen Y, Kelly J, Mariantoni M, Megrant A, O'Malley P, Sank D, Vainsencher A, Wenner J, White T, Yin Y, Cleland A N and Martinis J M 2012 *Nat. Phys.* **8** 719

[59] Mariantoni M, Wang H, Yamamoto T, Neeley M, Bialczak R C, Chen Y, Lenander M, Lucero E, O'Connell A D, Sank D, Weides M, Wenner J, Yin Y, Zhao J, Korotkov A N, Cleland A N and Martinis J M 2011 *Science* **334** 61

[60] Shalibo Y, Rofe Y, Shwa D, Zeides F, Neeley M, Martinis J M and Katz N 2010 *Phys. Rev. Lett.* **105** 177001

[61] O'Connell A D, Ansmann M, Bialczak R C, Hofheinz M, Katz N, Lucero E, McKenney C, Neeley M, Wang H, Weig E M, Cleland A N and Martinis J M 2008 *Appl. Rev. Lett.* **92** 112903

[62] Creedon D L, Reshitnyk Y, Farr W, Martinis J M, Duty T L and Tobar M E 2011 *Appl. Phys. Lett.* **98** 222903

[63] Steffen M, Ansmann M, McDermott R, Katz N, Bialczak R C, Lucero E, Neeley M, Weig E M, Cleland A N and Martinis J M 2006 *Phys. Rev. Lett.* **97** 050502

[64] Patel U, Gao Y, Hover D, Ribeill G J, Sendelbach S and McDermott R 2012 arXiv:1210.1545v1 [cond-mat.supr-con]

[65] Houck A A, Koch J, Devoret M H, Girvin S M and Schoelkopf R J 2009 *Quantum Inf. Process.* **8** 105

[66] Chen Y, Sank D, O'Malley P, White T, Barends R, Chiaro B, Kelly J, Lucero E, Mariantoni M, Megrant A, Neill C, Vainsencher A, Wenner J, Yin Y, Cleland A N and Martinis J M 2012 *Appl. Phys. Lett.* **101** 182601

[67] Wenner J, Barends R, Bialczak R C, Chen Y, Kelly J, Lucero E, Mariantoni M, Megrant A, O'Malley P J J, Sank D, Vainsencher A, Wang H, White T C, Yin Y, Zhao J, Cleland A N and Martinis J M 2011 *Appl. Rev. Lett.* **99** 113513

[68] Sandberg M, Vissers M R, Kline J S, Weides M, Gao J S, Wisbey D S and Pappas D P 2012 *Appl. Phys. Lett.* **100** 262605

[69] Neill C, Megrant A, Barends R, Chen Y, Chiaro B, Kelly J, Mutus J Y, O'Malley P J J, Sank D, Wenner J, White T C, Yin Y, Cleland A N and Martinis J M 2013 *Appl. Phys. Lett.* **103** 072601

[70] Gao J S, Daal M, Martinis J M, Vayonakis A, Zmuidzinas J, Sadoulet B, Mazin B A, Day P K and Leduc H G 2008 *Appl. Rev. Lett.* **92** 212504

[71] Megrant A, Neill C, Barends R, Chiaro B, Chen Y, Feigl L, Kelly J, Lucero E, Mariantoni M, O'Malley P J J, Sank D, Vainsencher A, Wenner J, White T C, Yin Y, Zhao J, Palmstrøm C J, Martinis J M and Cleland A N 2012 *Appl. Phys. Lett.* **100** 113510

[72] Vissers M R, Gao J, Wisbey D S, Hite D A, Tsuei C C, Corcoles A D, Steffen M and Pappas D P 2010 *Appl. Phys. Lett.* **97** 232509

[73] Wenner J, Yin Y, Lucero E, Barends R, Chen Y, Chiaro B, Kelly J, Lenander M, Mariantoni M, Megrant A, Neill C, O'Malley P J J, Sank D, Vainsencher A, Wang H, White T C, Cleland A N and Martinis J M 2013 *Phys. Rev. Lett.* **110** 150502

[74] Lenander M, Wang H, Bialczak R C, Lucero E, Mariantoni M, Neeley M, O'Connell A D, Sank D, Weides M, Wenner J, Yamamoto T, Yin Y, Zhao J, Cleland A N and Martinis J M 2011 *Phys. Rev. B* **84** 024501

[75] Sun L, DiCarlo L, Reed M D, Catelani G, Bishop L S, Schuster D I, Johnson B R, Yang G A, Frunzio L, Glazman L, Devoret M H and Schoelkopf R J 2012 *Phys. Rev. Lett.* **108** 230509

[76] Córcoles A D, Chow J M, Gambetta J M, Rigetti C, Rozen J R, Keefe G A, Rothwell M B, Ketchen M B and Steffen M 2011 *Appl. Rev. Lett.* **99** 181906

[77] Chow J M, Córcoles A D, Gambetta J M, Rigetti C, Johnson B R, Smolin J A, Rozen J R, Keefe G A, Rothwell M B, Ketchen M B and Steffen M 2011 *Phys. Rev. Lett.* **107** 080502

[78] Leghtas Z, Kirchmair G, Vlastakis B, Schoelkopf R J, Devoret M H and Mirrahimi M 2013 *Phys. Rev. Lett.* **111** 120501

[79] Leung D W, Nielsen M A, Chuang I L and Yamamoto Y 1997 *Phys. Rev. A* **56** 2567

[80] Fowler A G, Mariantoni M, Martinis J M and Cleland A N 2012 *Phys. Rev. A* **86** 032324

[81] Zhong Y P, Wang Z L, Wang H, Martinis J M, Cleland A N and Korotkov A N 2013 arXiv:1309.0198v1 [quant-ph]

[82] Lehnert K W, Bladh K, Spietz L F, Gunnarsson D, Schuster D I, Delsing P and Schoelkopf R J 2003 *Phys. Rev. Lett.* **90** 027002

[83] Wallraff A, Schuster D I, Blais A, Frunzio L, Huang R S, Majer J, Kumar S, Girvin S M and Schoelkopf R J 2004 *Nature* **431** 162

[84] Schuster D I, Wallraff A, Blais A, Frunzio L, Huang R S, Majer J, Girvin S M and Schoelkopf R J 2003 *Phys. Rev. Lett.* **94** 123602

[85] Wallraff A, Schuster D I, Blais A, Frunzio L, Majer J, Devoret M H, Girvin S M and Schoelkopf R J 2005 *Phys. Rev. Lett.* **95** 060501

[86] Reed M D, DiCarlo L, Johnson B R, Sun L, Schuster D I, Frunzio L and Schoelkopf R J 2010 *Phys. Rev. Lett.* **105** 173601

[87] Siddiqi I, Vijay R, Metcalfe M, Boaknin E, Frunzio L, Schoelkopf R J and Devoret M H 2006 *Phys. Rev. B* **73** 054510

[88] Lupaşcu A, Driessen E F C, Roschier L, Harmans C J P M and Mooij J E 2006 *Phys. Rev. Lett.* **96** 127003

[89] Lupaşcu A, Saito S, Picot T, de Groot P C, Harmans C J P M and Mooij J E 2007 *Nat. Phys.* **3** 119

[90] Mallet F, Ong F R, Palacios-Laloy A, Nguyen F, Bertet P, Vion D and Esteve D 2009 *Nat. Phys.* **5** 791

[91] Siddiqi I, Vijay R, Pierre F, Wilson C M, Metcalfe M, Rigetti C, Frunzio L and Devoret M H 2004 *Phys. Rev. Lett.* **93** 207002

[92] Vijay R, Devoret M H and Siddiqi I 2009 *Rev. Sci. Instrum.* **80** 111101

[93] Risté D, van Leeuwen J G, Ku H S, Lehnert K W and DiCarlo L 2012 *Phys. Rev. Lett.* **109** 050507